INSTITUTE OF PHYSICS PUBLISHING JOURNAL OF MICROMECHANICS AND MICROENGINEERING

J. Micromech. Microeng. **14** (2004) 1328–1336 PII: S0960-1317(04)75446-7

Spatial optimization of an array of aligned microcantilever based sensors

K Khanafer[1], A-R A Khaled[2] and K Vafai[1]

[1] Mechanical Engineering Department, University of California, Riverside, CA 92521, USA
[2] Mechanical Engineering Department, The Ohio State University, Columbus, OH 43210, USA

E-mail: vafai@engr.ucr.edu

Received 30 January 2004, in final form 12 May 2004
Published 13 July 2004
Online at stacks.iop.org/JMM/14/1328
doi:10.1088/0960-1317/14/10/006

Abstract

The present work establishes the optimized spatial arrangement for an array of aligned microcantilever sensors placed inside a fluidic cell. The results of the present investigation show that the optimum spacing distance between the microcantilevers decreases as the fluidic cell height decreases. An increase in the flow Reynolds number is found to increase the optimum spacing distance. However, this increase is not noticeable at relatively small Reynolds numbers where the flow exhibits creep characteristics. Hydromagnetic effects are found to decrease the optimum spacing distance. The results of the present investigation show that the location of the microcantilevers from the wall of the fluidic cell also plays a significant role on the optimum distance between the microcantilevers. Finally, a correlation for the optimum spacing distance between the microcantilevers is obtained for various pertinent parameters. This correlation can be used to determine the minimum size of biochips that will produce similar flow conditions on each microcantilever, resulting in independent microcantilever detections for different analytes.

Nomenclature

B	magnetic field strength (Tesla)
C	dimensionless analyte concentration
C'	analyte concentration ($g_{\text{analyte}}/g_{\text{solution}}$)
D	mass diffusivity of analyte ($\text{m}^2\ \text{s}^{-1}$)
H	dimensionless fluidic cell height
Ha	Hartmann number, $Ha = Bw\sqrt{\frac{\sigma}{\mu}}$
h	fluidic cell height (m)
L	dimensionless fluidic cell length
l	fluidic cell length (m)
P	dimensionless pressure
p	pressure (Pa)
Re	Reynolds number $Re = \frac{U_0 w}{\upsilon}$
S	dimensionless spacing between the microcantilevers
s	spacing between the microcantilevers (m)
Sc	Schmidt number $Sc = \frac{\upsilon}{D}$
U	dimensionless axial velocity
U_0	reference velocity ($\text{m}\ \text{s}^{-1}$)
u	dimensional axial velocity ($\text{m}\ \text{s}^{-1}$)
V	dimensionless normal velocity
υ	dimensional normal velocity ($\text{m}\ \text{s}^{-1}$)
W	dimensionless microcantilever width
w	microcantilever width (m)
X	dimensionless axial coordinate
x	dimensionless axial coordinate
Y	dimensionless normal coordinate
y	normal coordinate
Y_m	dimensionless location of the microcantilever from the wall
y_m	location of the microcantilever from the wall

Greek

μ	dynamic viscosity (Pa s)
ρ	fluid density ($\text{kg}\ \text{m}^{-3}$)
σ	electrical conductance of the fluid
υ	kinematic viscosity ($\text{m}^2\ \text{s}^{-1}$)

Subscripts

in quantity at the inlet
1 first species
2 second species

1. Introduction

The rapid growth of nanotechnology has led to new horizons for the development of microsensors that can be used to quickly detect, measure, analyze, and economically monitor chemical and biological agents in samples of a few microliters or less. The monitoring of a specific substance is pivotal in many applications ranging from clinical analysis to environmental control and for monitoring hazardous biological and chemical agents, toxins and chemical warfare agents. Microsensors could be used for clinical purposes in order to screen a patient for the presence of a disease or to determine its susceptibility to a given drug [1].

Microsensors containing microcantilevers are shown to be sensitive and accurate [1]. Changes in the physical properties of a microcantilever are used to detect changes in the environment surrounding it. Most often the deflection of the microcantilever is measured to indicate the presence or absence of a certain analyte. Microcantilevers are commonly made of silicon, silicon nitride, metal or combinations thereof.

For use in assays for biological or chemical agents, the microcantilevers are commonly a bimaterial, such as gold on one side and silicon on the other side. The gold side is then coated with a receptor that specifically binds to a given analyte (species being measured in an analytical procedure). Receptor/analyte pairs include antibodies and antigens, complementary nucleotide sequences and receptors and small molecules [2]. When the analyte molecules bind to the receptor, the side coated with the receptor will either become tensioned or relieved, thereby causing the microcantilever to deflect. The concentration of the analyte can be determined by the degree of deflection. The amount of deflection is usually in nanometers. This deflection is usually measured using optical techniques. Moreover, the detection of the microcantilever can be measured by monitoring its piezoelectric properties, which is a common method [3].

The concentration of the analyte on the microcantilever surface is mainly governed by the rate of the analyte adhesion to the receptor on the microcantilever surface as shown by Chang and Hammer [4]. This adhesion rate is usually a function of the analyte concentration in the vicinity of the microcantilever surface, the analyte rolling velocity at the receptor coated surface [5] and the rotational speed of the analyte molecules. The analyte rolling velocity is directly related to shear rates at the receptor surface. A model relating the pertinent parameters to the deflection of the microcantilever is illustrated in the work of Khaled *et al* [3].

Microsensors can be assembled into one fluidic device to form the so-called biochip. For example, a biochip can be a collection of microarrays such as DNA or protein microarrays arranged on a solid support or a biological IC chip [6]. Another example is the biochemo-opto-mechanical (BioCOM) chip illustrated in the works of Thundat *et al* [7]. Reliable detection for a biochip requires similar analyte adhesion rates on different microcantilever surfaces of the biochip collection if they are used to detect different analytes. This necessitates similar flow conditions in the vicinity of each microcantilever within the biochip.

The effect of a magnetic field normal to the flow of an electrically conducting fluid inside a channel is widely discussed in the literature (e.g. [8, 9]). Recently, hydromagnetic effects on oscillatory squeezed flows have been analyzed inside thin films by Khaled and Vafai [10]. They illustrated that hydromagnetic effects can reduce flow instabilities inside thin film fluidic cells associated with large squeezing effects. However, the literature lacks studies that relate hydromagnetic effects to the minimum spacing distance between aligned microcantilevers within a biochip, which results in full utilization of the microcantilevers. Moreover, hydromagnetic effects tend to reduce flow near the center of the fluidic cell [8–10]. This causes the flow exiting from the first microcantilever to travel over a smaller distance before resuming its fully developed flow stream profile. As such, the minimum spacing distance between aligned microcantilevers that ensures similar flow profiles over each can be reduced. This permits the utilization of more compact designs for biochips while maintaining equal detection capabilities.

In this work, flow and mass transfer over an array of similar microcantilevers are analyzed. The analysis establishes the minimum spacing distance between an array of the microcantilevers that produce similar flow conditions around each resulting in an optimum utilization of the biosensor. This minimum spacing distance is necessary for the microcantilevers to function independently of each other when they are used to detect concentrations of different analytes (species to be measured). Accordingly, a biochip with optimized dimensions can be constructed that possesses uniform flow conditions over each receptor surface. To achieve this objective, initially two microcantilevers will be used to establish the criterion for the optimum distance. This optimum spacing distance will then be generalized for arrays of multiple microcantilevers.

2. Mathematical formulation

Consider a two-dimensional, steady, incompressible flow through a fluidic cell having a length l and height h. The fluidic cell contains two microcantilevers aligned along the centerline of the fluidic cell and separated by a distance s. The physical model and coordinate system for such a fluidic cell are illustrated in figure 1. The microcantilevers are placed along the fluidic cell centerline. The analyte reacts with the receptor at the surface of the microcantilever. It is assumed in this investigation that the analyte is dilute and that the concentration does not affect the density. Furthermore, the Soret and Dufour effects are assumed to be negligible. In this investigation, the effect of a magnetic field of strength B on the flow where the fluid is assumed to be electrically conducting with an electrical conductance σ is investigated. This magnetic filed is assumed to be in y-direction so that it causes a resistance force in x-direction. The considered magnetic Reynolds number is very small so the induced Hall effect is negligible.

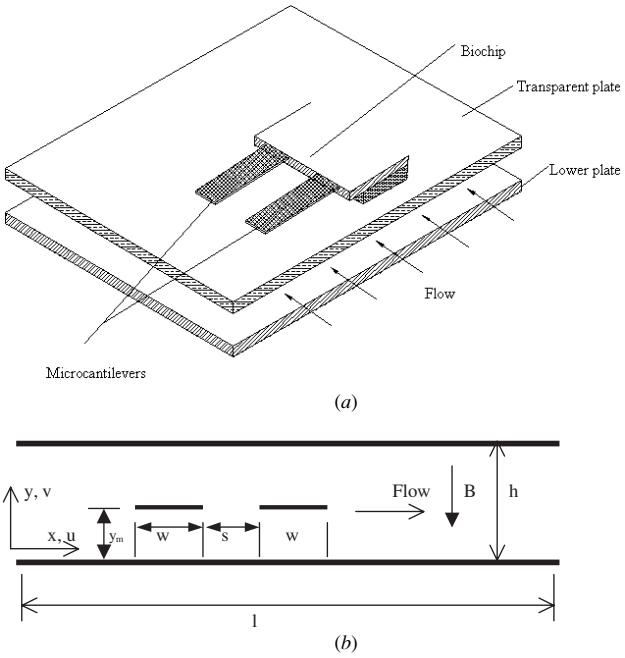

Figure 1. Schematic diagram and the corresponding coordinate system: (*a*) a three-dimensional view for a biochip, and (*b*) the front view with two microcantilevers in series.

The governing equations for the problem under investigation are based on the balance laws for mass, momentum, thermal energy and mass transport. Taking into account the above-mentioned assumptions, these equations are

$$\frac{\partial u}{\partial x}+\frac{\partial v}{\partial y}=0 \tag{1}$$

$$\rho\left(u\frac{\partial u}{\partial x}+v\frac{\partial u}{\partial y}\right)=-\frac{\partial p}{\partial x}+\mu\left(\frac{\partial^2 u}{\partial x^2}+\frac{\partial^2 u}{\partial y^2}\right)-\sigma B^2 u \tag{2}$$

$$\rho\left(u\frac{\partial v}{\partial x}+v\frac{\partial v}{\partial y}\right)=-\frac{\partial p}{\partial y}+\mu\left(\frac{\partial^2 v}{\partial x^2}+\frac{\partial^2 v}{\partial y^2}\right) \tag{3}$$

$$u\frac{\partial C_1'}{\partial x}+v\frac{\partial C_1'}{\partial y}=D_1\left(\frac{\partial^2 C_1'}{\partial x^2}+\frac{\partial^2 C_1'}{\partial y^2}\right) \tag{4}$$

$$u\frac{\partial C_2'}{\partial x}+v\frac{\partial C_2'}{\partial y}=D_2\left(\frac{\partial^2 C_2'}{\partial x^2}+\frac{\partial^2 C_2'}{\partial y^2}\right) \tag{5}$$

where C_1', C_2', u, v, ρ, p, μ, D_1 and D_2 are the concentration of the first species, the concentration of the second species, axial velocity, normal velocity, fluid density, pressure, average dynamic viscosity, mass diffusivity of the first species and the mass diffusivity of the second species, respectively. In our analysis, we are concerned with species that are very small compared to the fluidic cell height such that the mass transfer of the analyte molecules does not affect the flow of the main fluid. Equations (1)–(5) can be transformed into non-dimensional forms as follows,

$$\left.\begin{aligned} X=\frac{x}{w}\quad Y=\frac{y}{w}\quad (U,V)=\frac{(u,v)}{U_0}\\ C_1=\frac{C_1'-C_{1\,\mathrm{in}}'}{C_{10}'-C_{1\,\mathrm{in}}'}\quad C_2=\frac{C_2'-C_{2\,\mathrm{in}}'}{C_{20}'-C_{2\,\mathrm{in}}'}\quad P=\frac{pw}{\mu U_0}\end{aligned}\right\} \tag{6}$$

where C_{10}' and C_{20}' are reference concentrations for the considered species 1 and 2, respectively. The resulting non-dimensional governing equations are given by

$$\frac{\partial U}{\partial X}+\frac{\partial V}{\partial Y}=0 \tag{7}$$

$$U\frac{\partial U}{\partial X}+V\frac{\partial U}{\partial Y}=-\frac{1}{Re}\frac{\partial P}{\partial X}+\frac{1}{Re}\left(\frac{\partial^2 U}{\partial X^2}+\frac{\partial^2 U}{\partial Y^2}\right)-\frac{Ha^2}{Re}U \tag{8}$$

$$U\frac{\partial V}{\partial X}+V\frac{\partial V}{\partial Y}=-\frac{1}{Re}\frac{\partial P}{\partial Y}+\frac{1}{Re}\left(\frac{\partial^2 V}{\partial X^2}+\frac{\partial^2 V}{\partial Y^2}\right) \tag{9}$$

$$U\frac{\partial C_1}{\partial X}+V\frac{\partial C_1}{\partial Y}=\frac{1}{Sc_1 Re}\left(\frac{\partial^2 C_1}{\partial X^2}+\frac{\partial^2 C_1}{\partial Y^2}\right) \tag{10}$$

$$U\frac{\partial C_2}{\partial X}+V\frac{\partial C_2}{\partial Y}=\frac{1}{Sc_2 Re}\left(\frac{\partial^2 C_2}{\partial X^2}+\frac{\partial^2 C_2}{\partial Y^2}\right) \tag{11}$$

where Re, Ha, Pr and Sc are the Reynolds number, Hartmann number, Prandtl number and the Schmidt number, respectively. They are defined as

$$Re=\frac{U_0 w}{\upsilon},\quad Ha=Bw\sqrt{\frac{\sigma}{\mu}},\quad Pr=\frac{\upsilon}{\alpha},\quad Sc_1=\frac{\upsilon}{D_1}$$
$$\text{and}\quad Sc_2=\frac{\upsilon}{D_2}. \tag{12}$$

In the above equations, h, w, D_1, D_2 and υ are the height of the channel, width of the microcantilever, diffusion coefficient for the first species, diffusion coefficient for the second species and the kinematic viscosity, respectively. It should be noted that flow stream profiles become identical around the aligned microcantilevers for certain spacing distances. Under these conditions, both microcantilevers will function independently as if they are placed in separate fluidic cells as long as they are used to detect different analytes. This, in turn, ensures that both microcantilevers will have equal detection capabilities and that the second microcantilever can be fully utilized by maximizing the analyte flow rate over it.

The boundary conditions for the present study can be written as follows:

(1) *Inlet section*

$$X=0:\qquad U=6Y(H-Y),\ V=0,\ C_1=C_2=0. \tag{13}$$

(2) *Outlet section*

$$X=L:\qquad \frac{\partial U}{\partial X}=\frac{\partial V}{\partial X}=\frac{\partial C_1}{\partial X}=\frac{\partial C_2}{\partial X}=0. \tag{14}$$

(3) *Top and bottom walls*

$$\left.\begin{aligned} &Y=0, H \text{ and } 0\leqslant X\leqslant L:\\ &U=V=\frac{\partial C_1}{\partial Y}=\frac{\partial C_2}{\partial Y}=0\end{aligned}\right\} \tag{15}$$

where $H=h/w$, $L=l/w$ while the dimensionless spacing distance between the microcantilevers is S ($S=s/w$).

(4) *Microcantilever*. The boundary conditions along the lower surfaces of the available microcantilevers ($Y_m=y_m/w$) and along their edges are given by

$$\left.\begin{aligned} &\text{microcantilever 1, 2:}\qquad U=V=0,\\ &\frac{\partial C_1}{\partial n}=\frac{\partial C_2}{\partial n}=0.\end{aligned}\right\} \tag{16}$$

Over the upper surfaces of the utilized microcantilevers, analyte species binds with the receptor at these surfaces at a constant rate. This provides a sufficient tool for demonstrating the principle of self-independent microcantilevers detection through investigating both the velocity distribution and isoconcentration plots. That is, the boundary conditions at these surfaces are

$$\begin{aligned} &\text{microcantilever 1:} \quad U = V = 0, \quad \frac{\partial C_1}{\partial n} = 1 \\ &\text{microcantilever 2:} \quad U = V = 0, \quad \frac{\partial C_2}{\partial n} = 1. \end{aligned} \tag{17}$$

The velocity profile in the fully developed regions within the fluidic cell is obtained analytically by solving equation (8) in the absence of the convective terms. The result is as follows:

$$U(Y) = \frac{Ha(H/2)\cosh[Ha(H/2)]}{Ha(H/2)\cosh[Ha(H/2)] - \sinh[Ha(H/2)]} \times \left[1 - \frac{\cosh[Ha(H/2)(2Y/H-1)]}{\cosh[Ha(H/2)]}\right]. \tag{18}$$

It should be noted that increasing the flow rate by increasing the Reynolds number will increase the optimum spacing distance between the aligned cantilevers. This is because the flow exiting the first cantilever will reach the second cantilever at a higher speed as the flow rate increases. This causes the flow to travel over a larger distance before it will resume its fully developed conditions. With this spacing distance, mass transfer will be similar for each cantilever no matter which pair of analyte/receptor is investigated.

3. Numerical scheme

A finite element formulation based on the Galerkin method is employed to solve the governing equations subject to the initial and boundary conditions for the present study. The application of this technique is well described by Taylor and Hood [11] and Gresho *et al* [12] and its application is well documented [13]. The highly coupled and non-linear algebraic equations resulting from the discretization of the governing equations are solved using an iterative solution scheme using the segregated solution algorithm. The advantage of using this method is that the global system matrix is decomposed into smaller submatrices and then solved in a sequential manner. This technique results in considerably fewer storage requirements. The conjugate residual scheme is used to solve the symmetric pressure-type equation systems, while the conjugate gradient squared method is used for the non-symmetric advection–diffusion-type equations. A variable grid-size system is implemented in the present investigation especially near the walls and close to the microcantilevers to capture the rapid changes in the dependent variables. Extensive numerical experimentation is performed to attain grid-independent results for all the field variables. When the relative change in variables between consecutive iterations was less than 10^{-6}, convergence was assumed to have been achieved.

4. Validation

The present numerical method is benchmarked against four different numerical, analytical and experimental studies in the literature. The present numerical method is validated versus the works of Young and Vafai [14–16] for forced convective, incompressible flow in a channel with an array of heated obstacles. Comparison of the streamlines between the present solution and that of Young and Vafai [14] shows excellent agreement at various Reynolds numbers ($Re = 200$ and 800). As additional check on the accuracy of the present numerical scheme, the isotherms at $Re = 800$ also reveal that both results are in excellent agreement. These comparisons are shown in figures 2 and 3. Moreover, the fully developed velocity in the presence of magnetic field is compared against the solution given in equation (18) for various Hartmann numbers as shown in figure 4. This comparison shows an excellent agreement. Also, the present numerical method is validated against the experimental results for the flow resistance inside microchannels in the absence of the microcantilevers which is reported in the literature by Park *et al* [17]. Figure 5 shows a comparison of the friction factor between the present study and the experimental results of Park *et al* [17] for various Reynolds numbers. This figure illustrates that our simulation results are in excellent agreement with the experimental results. As such, the utilized continuum model is expected to provide a reliable estimation for the optimum spacing distance.

5. Discussion

A wide range of pertinent parameters that significantly affect the minimum spacing between an array of two microcantilevers are analyzed in the present investigation. These parameters include Reynolds number and the height of the fluidic cell. The ranges of these parameters are varied as $0.01 < Re < 3$ and $2 < H < 15$.

Figure 6 shows the effects of both the flow Reynolds number and the dimensionless height of the fluidic cell on the optimum spacing distance between the aligned microcantilevers. Fluidic cells with relatively lower heights usually attain their fully developed conditions at a shorter distance when compared to those with relatively larger heights. As such, flow exiting the first microcantilever reaches the fully developed state faster as the height of the fluidic cell decreases as illustrated in figure 6. The minimum spacing distances appearing in figure 6 correspond to the spacing distances that cause centerline velocities after the end of the first microcantilever to reach 99% of their fully developed condition before being disturbed by the second microcantilever.

As seen in figure 6, the optimum spacing distance between microcantilevers is almost independent of the Reynolds number for fluidic cells having relatively small heights. The flow within the selected range of the Reynolds numbers is mainly governed by viscous forces. At a larger Reynolds numbers or at relatively large fluidic cell height, inertial forces become more comparable with viscous forces altering the optimum spacing specification between the microcantilevers (figure 6).

Reducing the Reynolds number by reducing the flow speed causes a slow down in the transport of the analytes molecules. This results in a larger detection time. As such, it is preferred to have fluidic cells with smaller heights so that the optimum spacing distance between the microcantilevers

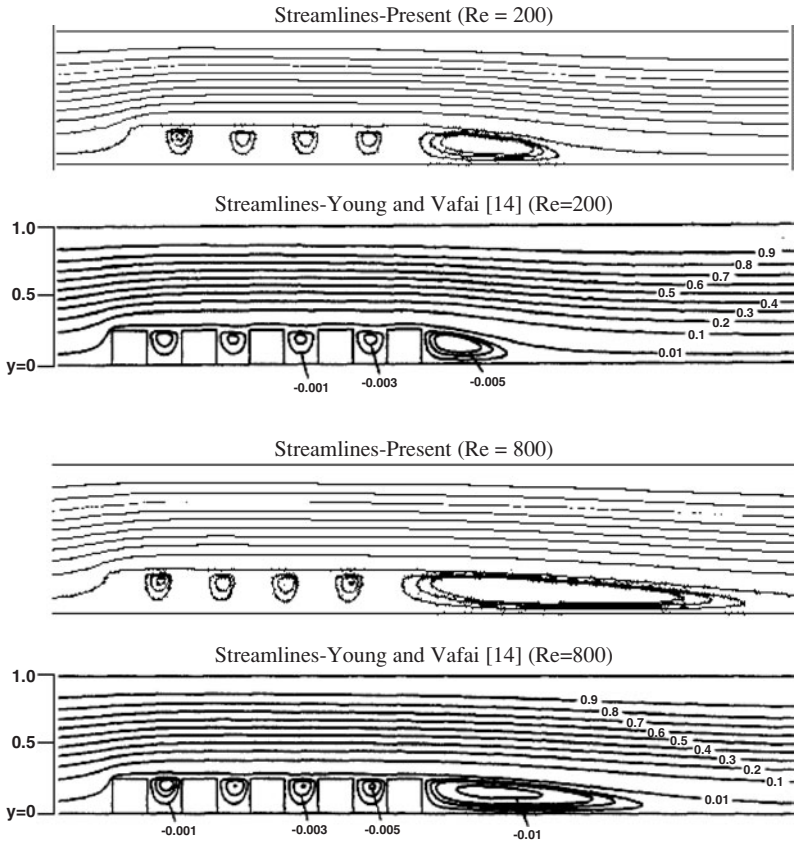

Figure 2. Comparison of the streamlines contours between the present numerical scheme and that of Young and Vafai [14] for $Re = 200$ and $Re = 800$.

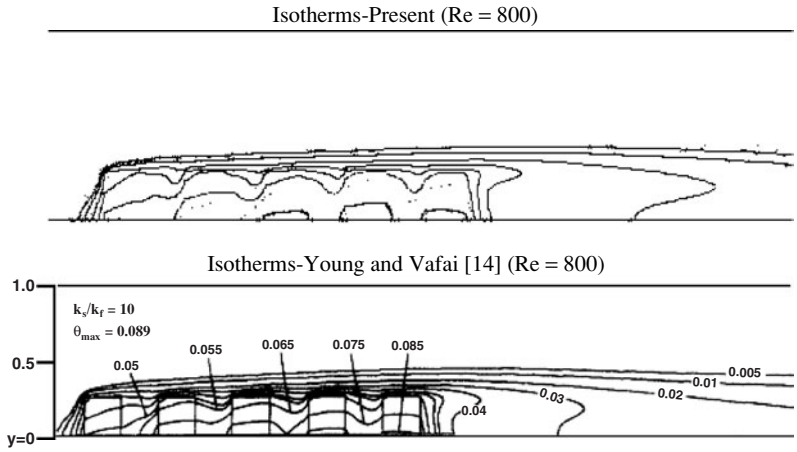

Figure 3. Comparison of the isotherms contours between the present numerical scheme and that of Young and Vafai [14].

is minimized and the transport of analyte molecules remains almost unaffected. However, velocity gradients and flow disturbances within fluidic cells increase as the fluidic cell heights decrease and accordingly the microcantilever detection becomes more sensitive to the location of the microcantilever. As such the noise associated with flow disturbances becomes an important consideration resulting in substantial errors in the measurements taken by the microcantilever.

Figure 7 illustrates the effects of the spacing distance between the microcantilevers on the centerline velocity within the fluidic cell for Reynolds number $Re = 2.5$ and fluidic cell height $H = 10$. As the dimensionless spacing distance between the microcantilevers increases from $S = 5$ to $S = 19.08$, the flow approaches its fully developed conditions before reaching the inlet section of the second microcantilever as shown in figure 7. At $S = 19.08$, the centerline velocity at the inlet of the second microcantilever is almost similar to that at the inlet section of the first microcantilever. This is necessary to achieve proper independent detection by microcantilevers. Moreover, velocity profiles at the inlet of the two microcantilevers

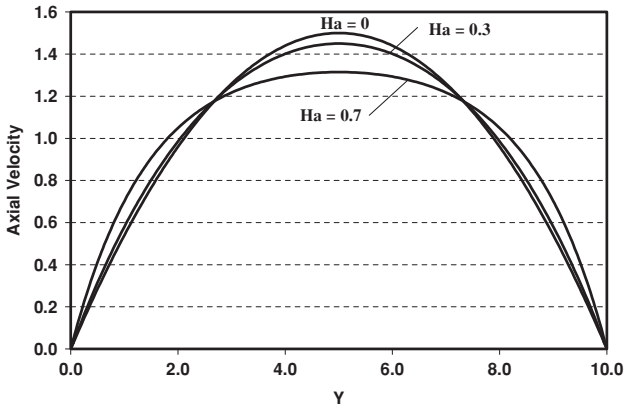

Figure 4. Comparison of the fully developed axial velocity within the fluidic cell between the present results and the analytical results for various Hartman numbers.

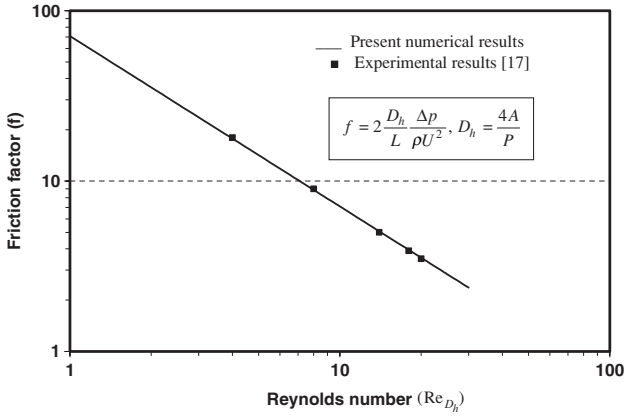

Figure 5. Comparison of the friction factor between the present study and that of Park *et al* [17] for various Reynolds numbers.

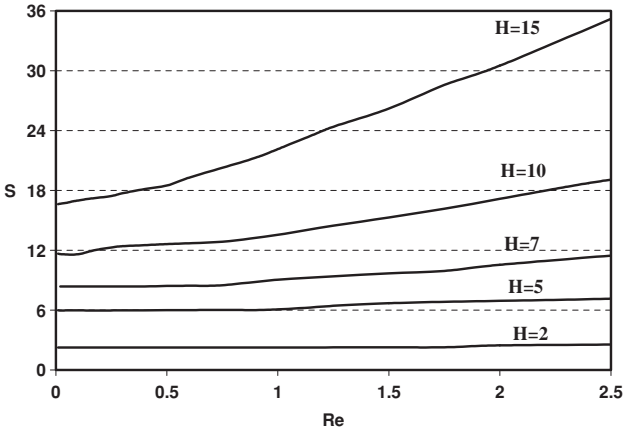

Figure 6. Effect of the Reynolds number on the optimum spacing between two microcantilevers for various fluidic cell heights ($Ha = 0$, $Y_m = H/2$).

are found to be almost identical for the optimum distance $S = 19.08$ as shown in figure 8. Again, this will enhance the detection performance of the microcantilevers.

It should be noted that the detection capability of a microcantilever is proportional to the analyte concentration along its surface. Independent detection by the

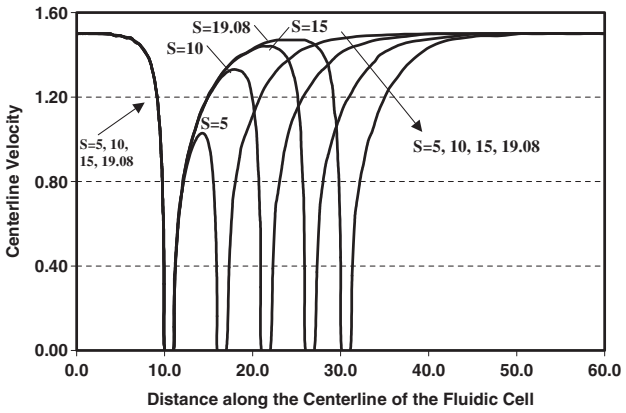

Figure 7. Effect of the spacing distance between the microcantilevers on the centerline velocity $U(X, H/2)$: $H = 10$, $Re = 2.5$, $Ha = 0$.

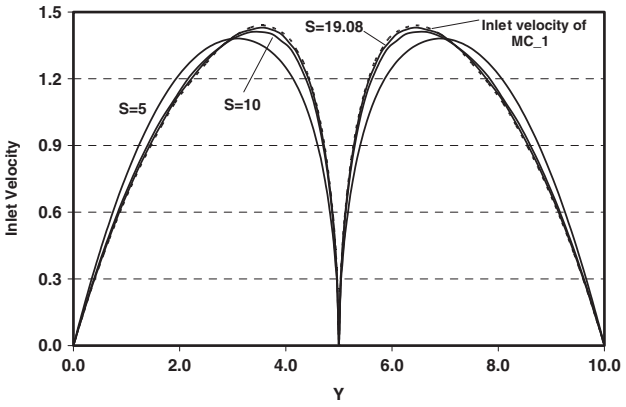

Figure 8. Effect of the spacing distance on the inlet velocity of the second microcantilever compared with the first microcantilever ($Re = 2.5$, $H = 10$, $Ha = 0$).

microcantilevers is achieved for the case beyond an optimum distance of $S = 19.08$ since the concentration on both microcantilevers is almost identical as illustrated in figure 9.

The effect of the spacing distance between the microcantilevers on the streamlines and the horizontal velocity contours for Reynolds number of $Re = 2.5$ and a fluidic cell height of $H = 10$ are shown in figures 10 and 11. Both figures show that a minimum spacing distance of $S = 19.08$ is required to achieve similar fully developed flow conditions at the inlet sections of both microcantilevers.

Hydromagnetic effects on the optimum spacing distance between the microcantilevers are shown in figure 12. A resistive force called the Lorentz force is generated against the flow when a magnetic field normal to the flow is applied on an electrically conducting fluid. This force tends to flatten the core of the velocity profile in the fluidic cell thus the distance needed for the centerline velocity to attain its fully developed condition is expected to decrease as the Hartmann number increases as seen in figure 12. This phenomenon is useful in constructing biochips since their size can be minimized using properly adjusted hydromagnetic effect.

The effect of varying the location of the microcantilevers from the centerline of a fluidic cell on the optimum spacing distance for various Reynolds numbers is shown in figure 13.

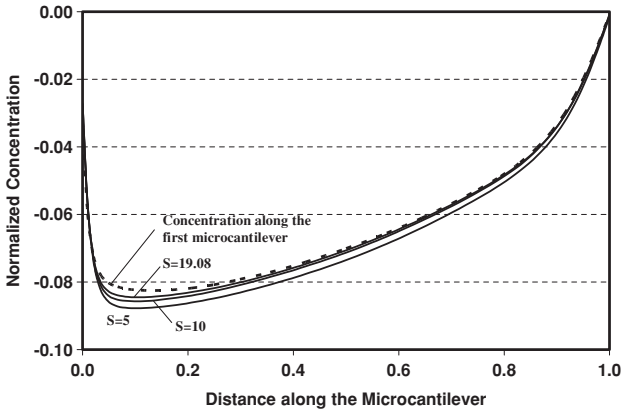

Figure 9. Effect of the spacing distance on the concentration distribution along the second microcantilever compared with the first microcantilever ($Re = 2.5$, $H = 10$, $Sc_1 = Sc_2 = 800$, $Ha = 0$).

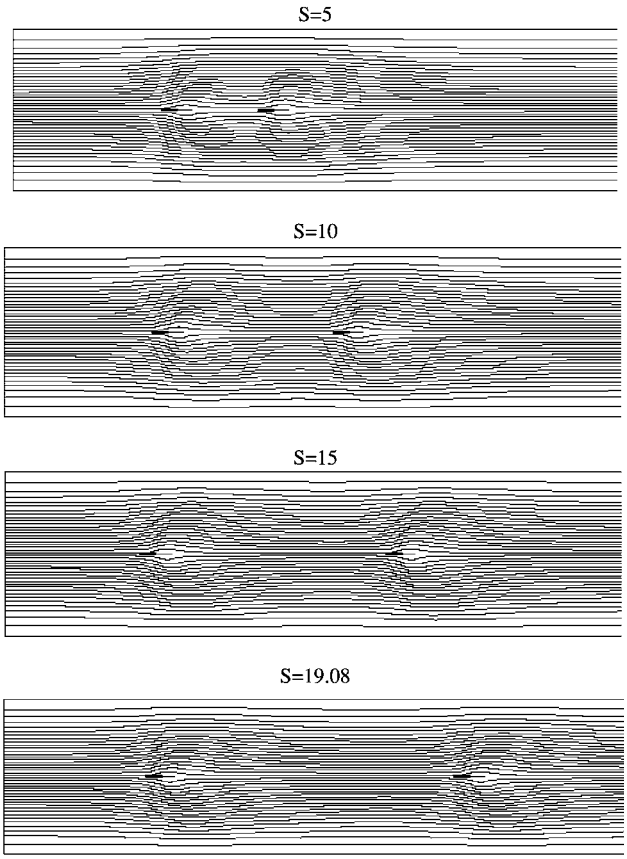

Figure 10. Effect of the spacing distance on the streamlines ($Re = 2.5$, $H = 10$, $Ha = 0$).

This figure shows that if the microcantilevers are placed closer to the solid wall of the fluidic cell, the optimum distance changes significantly as compared with the optimum distance associated with the microcantilevers placed along the centerline of the fluidic cell. This is due to the asymmetry in the flow distribution in the fluidic cell as a result of the presence of the microcantilevers. It changes the flow distribution regardless of where it is. The axial velocity decreases for $H/8$ and $H/16$ as shown in figure 14. As such, the flow disturbances which affect the detection process are minimized when microcantilevers are placed close to the wall.

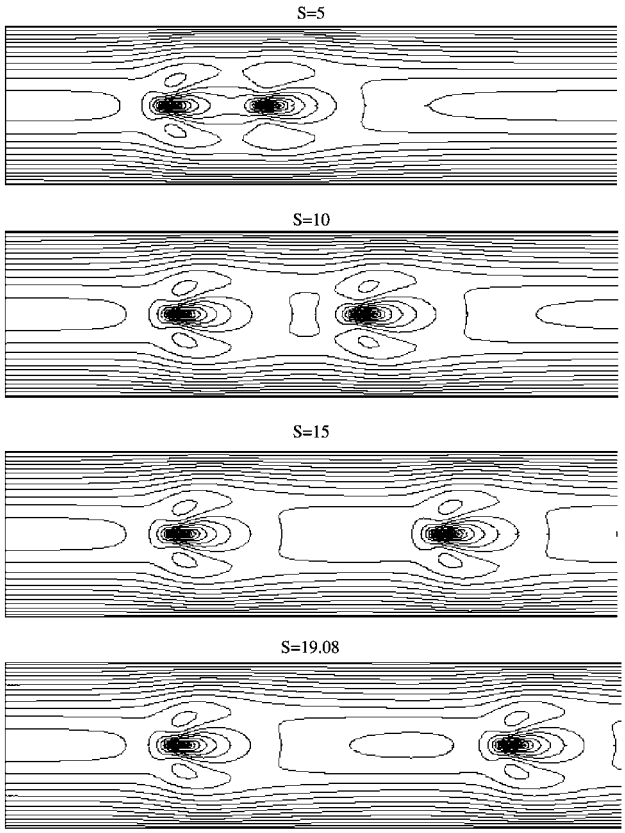

Figure 11. Effect of the spacing distance on the axial velocity ($Re = 2.5$, $H = 10$, $Ha = 0$).

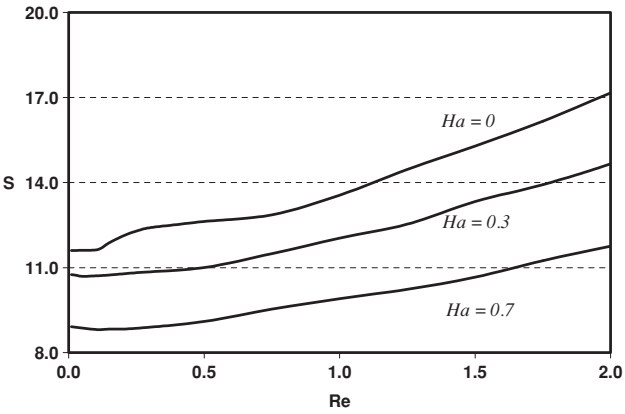

Figure 12. Effect of the Hartmann number on the optimum spacing distance between the microcantilevers ($H = 10$, $Y_m = H/2 = 5$).

Finally, the optimum spacing distance between an array of two microcantilevers is generalized for multiple microcantilevers as shown in figure 15. This figure shows that the optimum distance between two microcantilevers can be generalized for multiple microcantilevers to establish identical flow conditions. An example of this is shown in figure 15.

6. Optimum spacing correlation

For an optimum utilization of microcantilevers, the optimum distance between any two microcantilevers is correlated in terms of various pertinent parameters including Reynolds

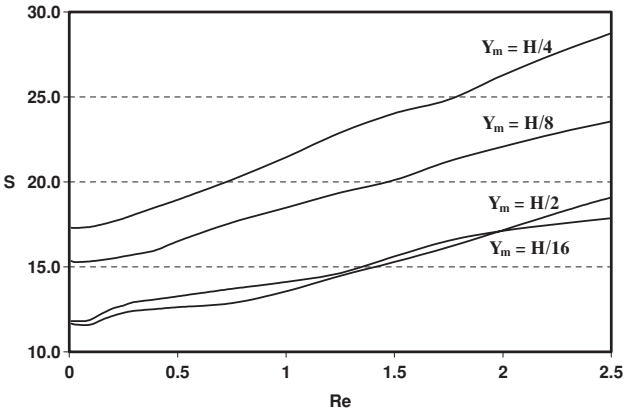

Figure 13. Effect of varying the location of the microcantilevers on the optimum spacing for various Reynolds number ($H = 10$, $Ha = 0$).

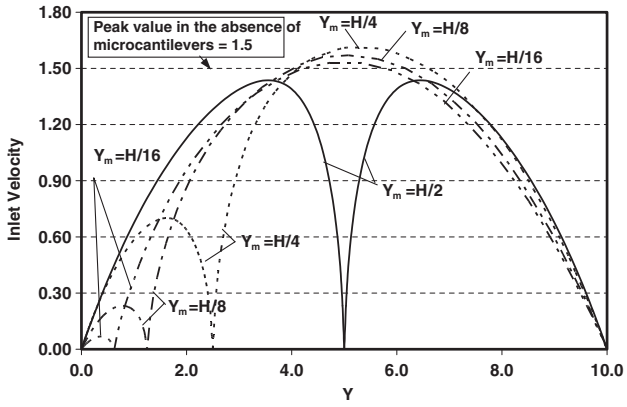

Figure 14. Effect of varying the location of the microcantilevers on the inlet velocity of the first microcantilever ($Re = 2.5$, $H = 10$, $Ha = 0$).

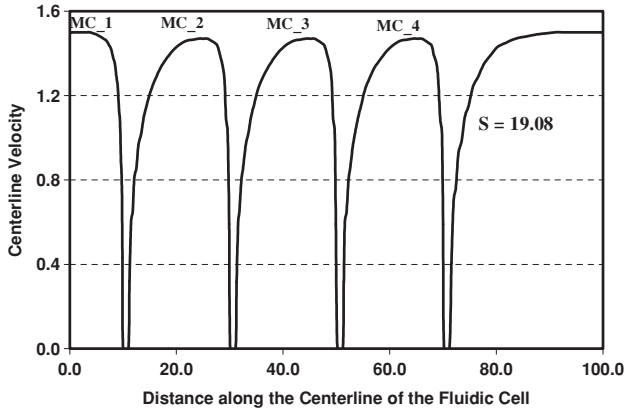

Figure 15. Effect of the spacing distance between an array of four microcantilevers on the centerline velocity $U(X, H/2)$: $H = 10$, $Re = 2.5$, $Ha = 0$, $Y_m = 5$.

number, the height of the fluidic cell and the location of the microcantilevers from the wall. This correlation can be written as follows,

$$\frac{S}{Y_m} = -1.8867 + 2.2468\left(\frac{H}{Y_m}\right) - 0.0573\left(\frac{H}{Y_m}\right)^2$$

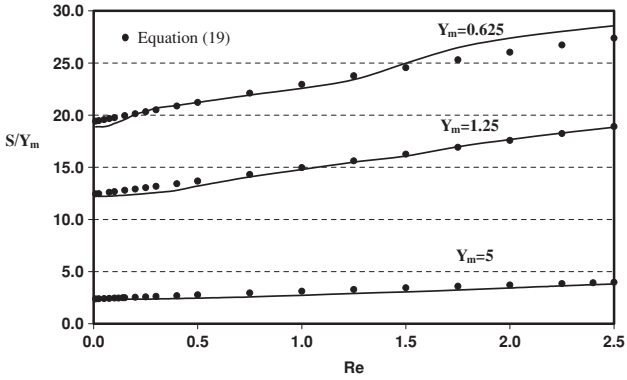

Figure 16. Comparison of the microcantilevers optimum spacing distance between the present numerical results and equation (19) for various elevations of the microcantilever ($H = 10$).

$$+ 0.1238\,Re - 0.1692\,Re^2 + 0.3686\left(\frac{H}{Y_m}\right)Re$$
$$- 8.64 \times 10^{-3}\left(\frac{H}{Y_m}\right)^2 Re + 0.0547\left(\frac{H}{Y_m}\right)Re^2$$
$$- 3.7099 \times 10^{-3}\left(\frac{H}{Y_m}\right)^2 Re^2 \qquad (19)$$

where the confidence coefficient of the above equation is $R^2 = 98.5\%$. The above correlation is obtained over the following range of parameters: $2 < H < 15$, $0.01 < Re < 2.5$, $H/16 > Y_m > H/2$. The obtained correlation for the optimum spacing distance is valuable for researchers using microsensors as it guides them to design highly accurate and efficient microsensor systems. Moreover, a graphical representation of the above correlation is shown in figure 16 for various values of fluidic cell heights. This figure shows an excellent agreement between the present numerical results and those obtained by the correlation.

7. Conclusions

An investigation of the optimum spatial arrangement for an array of microcantilevers in a fluidic cell is presented in this work based on a comprehensive flow and mass transfer analysis. The optimum spacing between the microcantilevers is established for achieving independent detections by the microcantilevers. The governing continuity, momentum and mass transfer equations are non-dimensionalized and solved based on a Galerkin method of weighted residuals. Effects of a wide range of pertinent parameters, such as Reynolds number and the height of the fluidic cell, are thoroughly investigated.

Different criteria are used to determine the optimum spacing distance between microcantilevers. This is accomplished through monitoring the centerline velocity along the fluidic cell length, matching up the velocity profiles at the inlet sections of the microcantilevers, comparing the local variation of the analyte concentrations along each microcantilever surface and monitoring the streamlines around the microcantilevers. The results of the present work show that the optimum spacing between the microcantilevers decreases as both the fluidic cell height and the Reynolds number decrease. Also, it was found that optimum spacing becomes

independent of the Reynolds number for relatively small values of the Reynolds number where the flow is characterized as a creep flow. The results of the present study show that the established criterion for independent detection of two microcantilevers is valid for multiple microcantilevers. Finally, an effective design correlation for the optimum spacing is obtained to determine the effective size of biochips for achieving independent microcantilever detection.

Acknowledgment

We acknowledge support for this work by DOD/DARPA/DMEA under grant no DMEA90-02-2-0216.

References

[1] Wu G, Ji H, Hansen K, Thundat T, Datar R, Cote R, Hagan M F, Chakraborty A K and Majumdar A 2001 Origin of nanomechanical cantilever motion generated from biomolecular interactions *Proc. Natl Acad. Sci. USA* **98** 1560–4

[2] Raiteri R, Nelles G, Butt H-J, Knoll W and Skladal P 1999 Sensing of biological substances based on the bending of the microfabricated cantilevers *Sensors Actuators* B **61** 213–7

[3] Khaled A-R A, Vafai K, Yang M, Zhang X and Ozkan C S 2003 Analysis, control and augmentation of microcantilever deflections in bio-sensing systems *Sensors Actuators* B **94** 103–15

[4] Chang K-C and Hammer D A 1999 The forward rate of binding of surface-tethered reactants: effect of relative motion between two surfaces *Biophys. J.* **76** 1280–92

[5] Pritchard W F, Davis P F, Derafshi Z, Polacek D C, Tsoa R, Dull R O, Jones S A and Giddens D P 1995 Effects of wall shear stress and fluid recirculation on the localization of circulating monocytes in a three dimensional flow model *J. Biomech.* **28** 1459–69

[6] Vo-Dinh T, Cullum B M and Stokes D L 2001 Nanosensors and biochips: frontiers in biomolecular diagnostics *Sensors Actuators* B **74** 2–11

[7] Thundat T, Wu G, Mao M and Majumdar A 1999 Biochemo-opto-mechanical (BioCOM) chip for chemical and biomolecular detection *First NASA and NCI Workshop on Sensors for Bio-Molecular Signatures*

[8] Hunt J C R 1965 Magnetohydrodynamic flow in rectangular ducts *J. Fluid Mech.* **21** 577–90

[9] Alty C J N 1971 Magnetohydrodynamic duct flow in a uniform magnetic field of arbitrary orientation *J. Fluid Mech.* **48** 429

[10] Khaled A-R A and Vafai K 2003 Heat transfer and hydromagnetic control of flow exit conditions inside oscillatory squeezed thin films *Numer. Heat Transfer* A **43** 239–58

[11] Taylor C and Hood P 1973 A numerical solution of the Navier-Stokes equations using finite-element technique *Comput. Fluids* **1** 73–89

[12] Gresho P M, Lee R L and Sani R L 1980 On the time-dependent solution of the incompressible Navier-Stokes equations in two and three dimensions *Recent Advances in Numerical Methods in Fluids* (Swansea: Pineridge)

[13] *FIDAP Theoretical Manual* 1990 (Evanston, IL: Fluid Dynamics International)

[14] Young T and Vafai K 1998 Convective flow and heat transfer in a channel containing multiple heated obstacles *Int. J. Heat Mass Transfer* **41** 3279–98

[15] Young T and Vafai K 1998 Convective cooling of a heated obstacle in a channel *Int. J. Heat Mass Transfer* **41** 3131–48

[16] Young T and Vafai K 1999 An experimental investigation of forced convective characteristics of arrays of channel mounted obstacles *ASME J. Heat Transfer* **121** 34–42

[17] Park H, Pak J J, Son S Y, Lim G and Song I 2002 Fabrication of a microchannel integrated with inner sensors and the analysis of its laminar characteristics *Sensors Actuators* A **103** 317–29